

Original Article

# Bond Strengthening of Unbonded RC Beams with the Advanced Carbon Fiber Reinforcement Polymer (CFRP) Composites

Fares Jnaid

Department of Civil Engineering, Fairleigh Dickinson University, New Jersey, USA

Received: 05 January 2022

Revised: 08 February 2022

Accepted: 19 February 2022

Published: 28 February 2022

**Abstract** - Confinement of concrete increases the bond between steel rebars and the surrounding concrete. This paper studies the effects of Carbon Fiber Reinforcement Polymer CFRP confinement in increasing the bond strength of concrete beams with unbonded reinforcement. The author developed a Finite Element (FE) model and verified it against the experimental data. In addition, the author developed an innovative numerical, analytical procedure to compute the strength of concrete beams with unbonded reinforcement and strengthened with CFRP sheets. The author subjected the beams to unbonded lengths that varied from 0 to full span and observed the mode of failure. Beams that failed in bond were wrapped with CFRP sheets in order to increase the bond between steel reinforcement and the surrounding concrete. This research concluded that wrapping beams with CFRP sheets restored up to 93% of ultimate capacity and increased the mid-deflection by up to 73%. In some cases, CFRP sheets were able to switch the mode of failure from an undesirable bond failure to a more attractive flexural failure.

**Keywords** - Concrete, Beams, CFRP, Bond, Strengthening.

## 1. Introduction

Considerable numbers of structures are experiencing significant amounts of deterioration before reaching their design service life. This premature deterioration is considered a problem in terms of the structural integrity and safety of the structure. Moreover, the deterioration of infrastructure has a significant amount of costs associated with it. In many cases, the root of a deterioration problem is caused by corrosion of steel reinforcement in concrete structures [1] and [2]. Corrosion of steel in a reinforced concrete structure leads to cracking of the concrete cover, reduction of steel cross-sectional area, loss of concrete integrity, and loss of bond between steel bars and surrounding concrete. This reduces strength and ductility, which shortens the service life of the structure. Fig. 1 shows the consequences of corrosion on structural performance [3]. When external loads are applied on the concrete surface, a complete bond between the concrete member and the embedded rebars must be secured. This will make sure that the two materials act in a composite manner, ensure a complete transfer of tensile stresses from the concrete to the steel rebars, and guarantee a ductile structural behaviour [4].

## 2. Bond Vs Unbond

Bond is considered a force transfer mechanism according to the ACI Building Code Requirements for Structural Concrete and Commentary [5]. A perfect bond between the steel reinforcement and the surrounding concrete is essential to ensure a complete transfer of stresses and

allow the structural member to reach its design strength[6-9][9]. The tensile stress transfer from concrete to the embedded steel rebars is shown in Fig. 2. Note that Fig. 2. ignores the vertical stress variation as it is a function of the distance to the neutral axis.

The bond deterioration between steel bars and the surrounding concrete is caused by the breakdown of the passive layer on the surface of the steel reinforcement. When rebar corrodes, its volume initially increases by a factor of 8 to 12 times the original volume of the rebar. As a result, it produces extremely large radial stresses on the concrete. When the internal radial stresses exceed the tensile strength of concrete, cracks form between the corroded rebar and the closest exterior surface. As the corrosion advances, it significantly decreases the size and the yield strength of the rebar. In addition to the loss of cross-sectional area and mechanical properties, rebar corrosion destroys the bond between the rebar and the surrounding concrete, allowing the steel to slip within the concrete. This results in a significant decrease in the ability of the rebar to transfer forces as the cross-section fails to behave in a composite manner (Fig. 3).

The Building Code Requirements for Structural Concrete [5] requires a flexural ductile mode of failure when designing concrete beams, i.e., crushing of concrete at the extreme compression fibres preceded by yielding of steel reinforcement at the tension side of the cross-section, while the beam exhibits large ductility. With the absence of stress



transfer from the concrete to the steel rebars due to loss of bond, the above ductile mode of failure cannot be achieved. on the contrary, a thin sudden bond failure will occur. Moreover, The ACI design equations of the statically indeterminate concrete cross-section are based on the compatibility of deformations. In other words, the strain in steel rebars is assumed to be equal to that in the adjacent concrete. This assumption is valid due to the perfect bond between the steel rebars and the surrounding concrete. A loss of bond will allow a steel slip within the concrete beam; consequently, strain compatibility is no longer guaranteed, and the code equations for flexural design are impractical.

### 3. Background

Despite the fact that the behaviour of unbonded beams has been examined since the mid-1970s [10-19], the conducted research addressing the above subject has been limited and failed to investigate the behaviour of unbonded beams [20].

#### 3.1. Experimental Research on Unbond

Minkarah and Ringo [10] revealed that while beams with an unbonded length of 60% of the span experienced approximately 20% reduction in flexural strength, beams with an unbonded length of less than 20% of the span length showed no reduction in ultimate flexural strength. This reduction in ultimate flexural strength is attributed to the reduction in strain, which is caused by the unbond between steel and concrete [12, 17, 19]. Based on the results of testing, 19 RC beams with different reinforcement ratios and various unbonded lengths, Cairns and Zhao [11] reported up to 50% loss in ultimate flexural strength with an unbonded length of 90% of span length and relatively large reinforcement ratios. The above conclusions were confirmed by Raoof and Lin [12] After testing a total of 44 small-scale beams and 88 large-scale beams. Further, Kotsovos *et al.* [20] suggested that unbond over full length causes sudden premature failure, so did Eyre and Nokhasteh [21] when they suggested that beams with large unbonded lengths are subject to sudden failure without yielding steel reinforcement. Du *et al.* [18] suggested that unbond changes the mode of failure of concrete beams in addition to reducing their flexural strength.

Despite the amount of experimental research performed on unbond, these experiments avoided exposing the studied beams to bond failure. This was performed by securing the bond between concrete and steel rebars either by providing hooks at rebar ends [11, 12, 21] (Fig. 4a), welding the rebars ends to steel plates in order to provide anchorage [20] (Fig. 4b), or by applying a relatively short unbonded length in order to prevent a bond failure [10, 16] as shown in Fig. 4c. In other words, the above researchers studied the effects of unbond on reducing the ultimate flexural strength rather than the effects of unbond on switching the mode of failure from flexural mode of failure to bond mode of failure.

#### 3.2. Numerical Research on Unbond

In addition to experimental studies, the behaviour of RC beams with unbonded reinforcement has been investigated by using Finite Element Analysis (FEA) [21-24, 11]. Multiple FEA packages have been utilized, such as ANSYS, DIANA, ABAQUS and MIDAS FEA. Further, the above researchers connected steel rebars and concrete elements to the same node when modelling the bond between steel rebars and surrounding concrete; this procedure will guarantee a zero slip between steel rebars and the adjacent concrete while the analysis is performed, which, in turn, will eliminate a bond or anchorage failure (Fig. 5). Wang and Chen [22] suggested that the length of unbonded rebars does not affect the strength of concrete beams. This is because the modelled beams were very lightly reinforced, which maintained the yield strain in the exposed bars despite strain reduction due to unbond. on the other hand, Eyre and Nokhasteh [21] observed that the mode of failure of concrete beams with short debonded lengths is similar to that in under reinforced beams. However, when the exposed length is large enough, the failure mode is more comparable to over reinforced beams. This was later confirmed by Cairns and Zhao [11]. This is also because the modeled beams did not experience any bond failure as the steel rebars and concrete elements in the above models shared the same nodes. This means that the relative displacement between the corner of the concrete cuboid element and the steel spar sharing the same node is restricted. In other words, no slip between concrete beams and embedded rebars were permitted. The later modeling technique prevents longitudinal and transversal translation between steel rebars and the surrounding concrete and, thus, eliminates a bond failure.

Conversely, parallel to the experimental research, the numerical studies examined the effects of corrosion/unbond on decreasing the flexural capacity rather than studying the effects of unbond on flexural behaviour.

### 4. Bond Strengthening of Concrete Beams using CFRPS Sheets

Many factors affect the bond between steel rebars and concrete. The bond force increases with the increase of concrete compressive strength and with the confinement of concrete [25]. Confinement of concrete increases the ductility and compressive strength of concrete and is accomplished by wrapping the concrete in the direction perpendicular to the compressive/tensile stresses. Having flat surfaces, plates or sheets, CFRP systems are ideal for maintenance and retrofit applications on concrete components. FRP systems have very high tensile strength. They could simply be classified as a form of tension reinforcement, e.g. steel reinforcing bars. In addition, they are ideal for confining concrete members.

The primarily three categories that control the bond stress-slip behaviour are structural characteristics, properties

of reinforcing bars, and properties of concrete. Structural characteristics are explained by the geometrical arrangement of the reinforcement, which contains the following: bar spacing, development length, concrete cover, concrete confinement degree, and lap splices. Properties of reinforcing bars contain the bar diameter and location, yield stress of the steel, and roughness of the bar surface. Properties of concrete include tensile and compressive strength, aggregate type and size, consolidation degree, workability of concrete, slump, admixtures, and consolidation degree [25]. Confinement of concrete increases the bond strength, and as a result, it modifies the bond stress–slip relationship as it shifts the splitting mode of failure to a pullout failure. This is because confinement of concrete plays a major role in reducing the deterioration of post bond failure, which delays and controls crack propagation when compared to unconfined concrete. Moreover, bond stress/force is directly dependent on the concrete compressive strength; therefore, an increase in concrete compressive strength will necessarily cause an increase in the bond strength.

### 5. Research Significance

Despite the considerable amount of researchers who investigated the effects of unbond on concrete beams, their main focus was on the ultimate flexural strength of the beam rather than ductility. Moreover, the above researchers did not study the effects of loss of bond between steel reinforcement and the adjacent concrete on switching the mode of failure from a ductile flexural failure to a premature thin bond failure. Hence, there is a lack of research in the employment of FRP composites in eliminating the bond failure in steel-reinforced concrete beams. Corrosion of steel rebars deteriorates the bond between the concrete beam and the embedded rebars, which increases the risk of a sudden bond failure. This paper aims at investigating the increase of bond between steel reinforcement and the surrounding concrete by confining the concrete beam with CFRP. This increases the strength and ductility of the beam and eliminates a potential catastrophic bond failure.

### 6. FEA Model

The author used the commercial software ANSYS Mechanical APDL to conduct this research. The author used elements SOLID65, SOLID185, and LINK180 to model concrete, FRP sheets, and steel rebars, respectively. In addition, spring elements COMBIN39 and COMBIN14 modelled the bond and unbond between steel rebars and the surrounding concrete, respectively. Detailed material properties are presented in Appendix A

#### 6.1. Modelling of Unbond

In order to model the unbond, the author duplicated the concrete nodes in areas of unbond, connected the steel rebars to the new identical nodes, and then connected the coincident nodes with high stiffness linear vertical springs (COMBIN14). This allows the steel and concrete elements to

move freely horizontally while it forces them to move jointly along the vertical axis, as shown in Fig. 6a.

#### 6.2. Modelling of Bond

Whether confined with steel or FRP composites, bond stress–slip behavior of concrete confined with FRP or steel has been investigated by several researchers [26-37]. The most common bond stress–slip constitutive curves are those suggested by Harajli [31] and FIB Model Code [33]. The author modelled the bond between steel rebars and the adjacent concrete using the same approach of modelling unbond. However, in addition to the vertical spring elements (COMBIN14), dimensionless horizontal spring elements (COMBIN39) were inserted into the same nodes. The vertical springs were added, as shown in Fig. 6b. The author adopted the FIB Model Code for Concrete Structures [33] in order to model the bond between steel rebars and the surrounding concrete. The author generated the stress–slip curve for the above nonlinear horizontal spring elements based on Eq.2-Eq and table are shown in Appendix B.

The author created the aforementioned curves for unconfined and confined concrete, assuming that no split failure occurred when concrete was confined. In order to input the load–displacement curve of the COMBIN39 spring element as required by ANSYS, the author converted the stress into force by multiplying it by the surface area of the rebar between two nodes (Eq. 1).

$$P = \tau \frac{\pi d_0^2}{4} l_e \quad (\text{N}) \tag{Eq. 1}$$

where  $\tau$  is the bond stress,  $d_0$  is the bar diameter, and  $l_e$  is the element length in ANSYS.

FIB Model Code [33] presents two curves to define the bond stress–slip response of ribbed rebars embedded in confined concrete based on the mode of failure. The model presents the bond stress as a function of the relative longitudinal displacement  $s$  and suggests the following equations to plot the bond stress–slip curve (MPa).

$$\tau = \tau_b \left(\frac{s}{s_1}\right)^a \quad (\text{MPa}) \quad 0 < s < s_1 \tag{Eq. 2}$$

$$\tau = \tau_b \quad (\text{MPa}) \quad s_1 < s < s_2 \tag{Eq. 3}$$

$$\tau = \tau_b - (\tau_b - \tau_{bf}) \frac{s - s_2}{s_3 - s_2} \quad (\text{MPa}) \quad s_2 < s < s_3 \tag{Eq. 4}$$

$$\tau = \tau_{bf} \quad (\text{MPa}) \quad s_3 < s \tag{Eq. 5}$$

$$\tau_{b,split} = \eta_2 6.5 \left(\frac{f'_c}{25}\right)^{0.25} \left(\frac{25}{d_b}\right)^{0.2} \left[\left(\frac{c_{min}}{d_b}\right)^{0.25} \left(\frac{c_{max}}{c_{min}}\right)^{0.1} + k_m k_{tr}\right] \quad (\text{MPa}) \tag{Eq. 6}$$

where  $\tau_b$  and  $\tau_{b,split}$  Are the peak bond strength values for pull–out and splitting modes of failure, respectively. The parameters in the above equation are defined in Appendix B. The values in the first two columns, i.e., pullout failure, are

applicable for a well or suitably confined concrete. Depending on the mode of failure and confinement of concrete. The values in the next 4 columns (splitting failure) are derived from Eq. 6 where  $k_{tr} = 12$  for confined concrete and  $k_{tr} = 0.0$  in the case on unconfined concrete; and  $k_m = 0.02$  for confined concrete and  $k_m = 0.0$  in the case on unconfined concrete. The bond stress–slip relationships, however, could be depicted by one of the curves in Fig. 7.

### 6.3. Verification of the FEA Model

Since FEA is a numerical solution, the accuracy of the obtained solution is dependent on the element size, degree of tolerance, and the number of iterations. The total number of elements of each beam is be increased until satisfactory results are constantly obtained within an acceptable tolerance. In addition, the verification process measures the change in results as a response to the variation in certain important parameters, such as material properties and load step.

In order to verify the FEA model, the author compared the model to existing experimental data performed by other researchers [38], [39]. Figs 8-15 compare the load-deflection curves of the experimental beams to those obtained from the FEA analysis. The details and specifications of the tested beams are shown in the figures the table presented in Appendix C. In addition, Appendix C shows a statistical comparison between the results of the experimental data and those obtained from the FEA model.

Appendix C and Figs 8-15 show that the FEA model can predict the ultimate flexural strength and mid-span deflection at ultimate of concrete beams and concrete beams strengthened with FRP with good accuracy.

## 7. Effect of Unbond on Concrete Beam Behavior

The author utilized the FEA model to investigate the behaviour of reinforced concrete beams with unbonded reinforcement. This was accomplished by applying unbonded lengths ( $L_{ub}$ ) that varied from 0 to 100% of the span (Fig. 16b).

Note that even with an unbonded length of 100% of the span, the rebars still experienced some bond beyond the end supports as the total length of the tested beams is slightly larger than the span. The investigated beam has a total length of 3200 mm (125.9 in.), a span of 3000 mm (118.1 in.), a cross-section of 254 mm (10 in.) x 152 mm (5.98 in.), and is reinforced with 2No.15 (0.63 in.).

The dimensions of the tested beam and cross-sectional details are shown in Fig. 17. The results of the analysis are shown in Appendix E, and the load-deflection curves are plotted in Fig. 17.

One can observe from Fig. 17. that when the unbonded length is less than 2600 mm (102.4 in.), even though the steel reinforcement yielded, there is a slight decrease in flexural load carrying capacity and in mid-span deflection at ultimate. This is owed to the decrease in the strain in steel at ultimate as a result of the unbond between steel rebars and the adjacent concrete. When the unbonded length is larger than 2600 mm (102.4 in.), however, the beams experience a sharp decrease in both flexural strength and ductility. This is because the beams failed in bond before the steel reinforcement reached its yield strength. Moreover, Appendix D shows that when the unbonded length is larger, 2600 mm (102.4 in.), the strain in steel rebars at ultimate is less than the yield strain. Furthermore, Appendix D shows the crack pattern and the cracking of the extreme elements in compression at mid-span of all the cases studied. The wider cracks are attributed to the loss of bond as there is no stress transfer from the concrete elements to the steel reinforcement, which results in wider and fewer cracks when compared to the control beam.

Appendix E shows that there is no octahedron outline at extreme compression fibres at mid-span in BU30 at collapse. This indicates that the concrete was crushed at the extreme compression zone. However, BU28 and BU26 experienced some crushing of concrete prior to collapse despite the fact that the steel rebars did not reach their yield strength. Furthermore, Appendix D shows that the strain in steel is decreasing with the increase of unbonded length. This decrease is causing the strain in steel to remain within the elastic range when the failure occurs in BU26, BU28, and BU30.

## 8. Applications of CFRP Sheets on Unbonded Beams

The author applied CFRP to beams BU24, BU26, BU28 and BU30 in order to increase the bond between steel rebars and the surrounding concrete. One layer of CFRP with a thickness of 1 mm was installed around the cross-section in the transverse direction to apply confinement to the concrete elements in the bonded region, as shown in Fig. 16c. The properties of the CFRP sheets are based on the recommendations of the ACI 440.2R-17 [40] and are presented in Appendix A. The ultimate capacity and strain in steel at ultimate are presented in Appendix D.

Fig. 18 shows the load-deflection curve of all of the cases studied and concludes that wrapping the beams with CFRP sheets increased the strength of BU24, BU 26, BU28, and BU30 by 3, 3.5, 27, and 108%, respectively. Furthermore, the application of CFRP sheets was able to increase the strain in steel dramatically in all of the cases studied. In addition, CFRP sheets were able to force the steel rebars to yield prior to the failure of CF26. This increase in strain, however, did not cause the rebars to yield prior to failure in CF28 and CF30. Appendix D shows that the

applications of CFRP were able to restore 93, 92, 89, and 81% of the ultimate capacity of BU24, BU 26, BU28, and BU30, respectively. Furthermore, CFRP sheets were able to switch the mode of failure of BU26 from a bond failure to a flexural one. However, even though the CFRP sheets failed to convert the mode of failure from a bond failure to a flexural one in BU28 and BU30, they were able to increase the mid-span deflection by 10 and 74%, respectively.

### 9. Analytical Solution

In the absence of a bond, the flexural strength of concrete beams is a function of the whole beam rather than the cross-section. This is due to the incompatibility of deformations in the static analysis of the cross-section. Consequently, the strain in the steel at ultimate cannot be obtained by applying the conventional equations of equilibrium. The total elongation of the steel rebars in the unbonded region, however, is equivalent to this of the adjacent concrete and can be calculated from Eq. 7.

If the bond force is smaller than the yield force, a bond failure will occur prior to a flexural failure. In this scenario, the force in the steel bars will be equal to the bond force and can be obtained from Eq. 8. In order to analytically calculate the ultimate flexural strength in the aforementioned case, the author developed a numerical iterative procedure where the strain in the extreme compression fibres varies from 0 to

0.003, and the depth of the neutral axis varies from 0 to  $d$  (effective depth). Depending on the value of the ultimate compression strain, integration of the stress-strain diagram of the concrete will compute the force in the compression side of the cross-section.

If the total bond force, however, is larger than the steel yield force, a flexural mode of failure is expected. Nevertheless, the ultimate flexural strength will be slightly lower than this in a fully bonded beam. This is a result of the strain reduction in steel rebars due to unbond. The author developed an empirical moment reduction factor based on the outcome of the FEA analysis.

Fig. 19 explains the algorithm that the author adopted in writing the analytical procedure code. The author used a combination of Bracketing Bisection numerical iterative methods to obtain the ultimate flexural strength where the developed code compares the tension force to the compression force to verify that the difference between the two values is within the acceptable tolerance limit. Whereas Appendix D presents a statistical comparison between the analytical solution and the FEA results and shows that the analytical procedure is able to predict the ultimate flexural strength of beams with unbonded reinforcement and beams strengthened with CFRP sheets.

$$\varepsilon_{sub} \cdot L_{ub} = \int_0^L \varepsilon_{cx} dx \tag{Eq. 7}$$

$$T = N \cdot \tau_{max} \frac{\pi d_0^2}{4} \quad (\text{N}) \tag{Eq. 8}$$

$$C_s = A'_s \cdot f_{yc} \tag{Eq. 9}$$

$$C_s = A'_s \cdot E_s \cdot \varepsilon_{sc} \tag{Eq. 10}$$

$$C_c = \int_0^{\varepsilon_0 \frac{c}{\varepsilon_{cu}}} b \cdot f'_c \cdot \left[ 2 \cdot \frac{\varepsilon_{cu} \cdot \frac{\varepsilon}{c} - \left( \frac{\varepsilon_{cu} \cdot \frac{\varepsilon}{c} \right)^2}{\varepsilon_0} \right] d\varepsilon + \int_{\varepsilon_0 \frac{c}{\varepsilon_{cu}}}^c b \cdot f'_c \cdot \left[ 1 - 0.15 \cdot \left( \frac{\varepsilon_{cu} \cdot \frac{\varepsilon}{c} - \varepsilon_0}{\varepsilon_{cu} - \varepsilon_0} \right) \right] d\varepsilon - f'_c \cdot A'_s \cdot \left[ 2 \cdot \frac{\varepsilon_{sc}}{\varepsilon_0} - \left( \frac{\varepsilon_{sc}}{\varepsilon_0} \right)^2 \right] \quad (\text{N}) \tag{Eq. 11}$$

$$y = \frac{(c - d') \cdot f'_c \cdot A'_s \cdot \left[ 2 \cdot \frac{\varepsilon_{sc}}{\varepsilon_0} - \left( \frac{\varepsilon_{sc}}{\varepsilon_0} \right)^2 \right]}{\int_0^{\varepsilon_0 \frac{c}{\varepsilon_{cu}}} \varepsilon \cdot b \cdot f'_c \cdot \left[ 2 \cdot \frac{\varepsilon_{cu} \cdot \frac{\varepsilon}{c} - \left( \frac{\varepsilon_{cu} \cdot \frac{\varepsilon}{c} \right)^2}{\varepsilon_0} \right] d\varepsilon + \int_{\varepsilon_0 \frac{c}{\varepsilon_{cu}}}^c \varepsilon \cdot b \cdot f'_c \cdot \left[ 1 - 0.15 \cdot \left( \frac{\varepsilon_{cu} \cdot \frac{\varepsilon}{c} - \varepsilon_0}{\varepsilon_{cu} - \varepsilon_0} \right) \right] d\varepsilon - f'_c \cdot A'_s \cdot \left[ 2 \cdot \frac{\varepsilon_{sc}}{\varepsilon_0} - \left( \frac{\varepsilon_{sc}}{\varepsilon_0} \right)^2 \right]} \quad (\text{mm}) \tag{Eq. 12}$$

$$C_c = \int_0^{\frac{\varepsilon_0 c}{\varepsilon_{cu}}} b \cdot f'_c \cdot \left[ 2 \cdot \frac{\varepsilon_{cu} \cdot \frac{\varepsilon}{c} - \left( \frac{\varepsilon_{cu} \cdot \frac{\varepsilon}{c} \right)^2}{\varepsilon_0} \right] d\varepsilon + \int_{\frac{\varepsilon_0 c}{\varepsilon_{cu}}}^c b \cdot f'_c \cdot \left[ 1 - 0.15 \cdot \left( \frac{\varepsilon_{cu} \cdot \frac{\varepsilon}{c} - \varepsilon_0}{\varepsilon_{cu} - \varepsilon_0} \right) \right] d\varepsilon - f'_c \cdot A'_s \cdot \left[ 1 - 0.15 \cdot \left( \frac{\varepsilon_{sc} - \varepsilon_0}{\varepsilon_{cu} - \varepsilon_0} \right) \right] \quad (\text{N}) \quad \text{Eq. 13}$$

$$y = \frac{\int_0^{\frac{\varepsilon_0 c}{\varepsilon_{cu}}} \varepsilon \cdot b \cdot f'_c \cdot \left[ 2 \cdot \frac{\varepsilon_{cu} \cdot \frac{\varepsilon}{c} - \left( \frac{\varepsilon_{cu} \cdot \frac{\varepsilon}{c} \right)^2}{\varepsilon_0} \right] d\varepsilon + \int_{\frac{\varepsilon_0 c}{\varepsilon_{cu}}}^c \varepsilon \cdot b \cdot f'_c \cdot \left[ 1 - 0.15 \cdot \left( \frac{\varepsilon_{cu} \cdot \frac{\varepsilon}{c} - \varepsilon_0}{\varepsilon_{cu} - \varepsilon_0} \right) \right] d\varepsilon - (c - d') \cdot f'_c \cdot A'_s \cdot \left[ 1 - 0.15 \cdot \left( \frac{\varepsilon_{sc} - \varepsilon_0}{\varepsilon_{cu} - \varepsilon_0} \right) \right]}{\int_0^{\frac{\varepsilon_0 c}{\varepsilon_{cu}}} b \cdot f'_c \cdot \left[ 2 \cdot \frac{\varepsilon_{cu} \cdot \frac{\varepsilon}{c} - \left( \frac{\varepsilon_{cu} \cdot \frac{\varepsilon}{c} \right)^2}{\varepsilon_0} \right] d\varepsilon + \int_{\frac{\varepsilon_0 c}{\varepsilon_{cu}}}^c b \cdot f'_c \cdot \left[ 1 - 0.15 \cdot \left( \frac{\varepsilon_{cu} \cdot \frac{\varepsilon}{c} - \varepsilon_0}{\varepsilon_{cu} - \varepsilon_0} \right) \right] d\varepsilon - f'_c \cdot A'_s \cdot \left[ 1 - 0.15 \cdot \left( \frac{\varepsilon_{sc} - \varepsilon_0}{\varepsilon_{cu} - \varepsilon_0} \right) \right]} \quad (\text{mm}) \quad \text{Eq. 14}$$

$$C_c = \int_0^{\frac{\varepsilon_0 c}{\varepsilon_{cu}}} b \cdot f'_c \cdot \left[ 2 \cdot \frac{\varepsilon_{cu} \cdot \frac{\varepsilon}{c} - \left( \frac{\varepsilon_{cu} \cdot \frac{\varepsilon}{c} \right)^2}{\varepsilon_0} \right] d\varepsilon + \int_{\frac{\varepsilon_0 c}{\varepsilon_{cu}}}^c b \cdot f'_c \cdot \left[ 1 - 0.15 \cdot \left( \frac{\varepsilon_{cu} \cdot \frac{\varepsilon}{c} - \varepsilon_0}{\varepsilon_{cu} - \varepsilon_0} \right) \right] d\varepsilon \quad (\text{N}) \quad \text{Eq. 15}$$

$$y = \frac{\int_0^{\frac{\varepsilon_0 c}{\varepsilon_{cu}}} \varepsilon \cdot b \cdot f'_c \cdot \left[ 2 \cdot \frac{\varepsilon_{cu} \cdot \frac{\varepsilon}{c} - \left( \frac{\varepsilon_{cu} \cdot \frac{\varepsilon}{c} \right)^2}{\varepsilon_0} \right] d\varepsilon + \int_{\frac{\varepsilon_0 c}{\varepsilon_{cu}}}^c \varepsilon \cdot b \cdot f'_c \cdot \left[ 1 - 0.15 \cdot \left( \frac{\varepsilon_{cu} \cdot \frac{\varepsilon}{c} - \varepsilon_0}{\varepsilon_{cu} - \varepsilon_0} \right) \right] d\varepsilon}{\int_0^{\frac{\varepsilon_0 c}{\varepsilon_{cu}}} b \cdot f'_c \cdot \left[ 2 \cdot \frac{\varepsilon_{cu} \cdot \frac{\varepsilon}{c} - \left( \frac{\varepsilon_{cu} \cdot \frac{\varepsilon}{c} \right)^2}{\varepsilon_0} \right] d\varepsilon + \int_{\frac{\varepsilon_0 c}{\varepsilon_{cu}}}^c b \cdot f'_c \cdot \left[ 1 - 0.15 \cdot \left( \frac{\varepsilon_{cu} \cdot \frac{\varepsilon}{c} - \varepsilon_0}{\varepsilon_{cu} - \varepsilon_0} \right) \right] d\varepsilon} \quad (\text{mm}) \quad \text{Eq. 16}$$

$$M_n = C_c \cdot (d - c + y) + C_s \cdot (d - d') \quad \text{Eq. 17}$$

$$\mu = 1.03e^{-0.18 \left( \frac{L_{ub}}{L} \right)} \quad \text{Eq. 18}$$

$$\mu = 1.3e^{-0.425 \left( \frac{L_{ub}}{L} \right)} \quad \text{Eq. 19}$$

## 10. Summary and Conclusion

This research investigated the effectiveness of CFRP sheets in strengthening the bond between steel rebars and the surrounding concrete. The author applied various lengths of

unbond between steel rebars and the adjacent concrete. The beams that experienced a decrease in strength were wrapped with CFRP sheets in the bonded region to increase the bond. The author developed a Finite Element model to simulate the

behaviour of beams with unbonded reinforcement and beams strengthened with CFRP sheets. In addition, the author developed an innovative analytical technique to calculate the ultimate flexural strength of beams strengthened with CFRP sheets.

The author drew the following conclusions:

Both FEA and analytical models were able to predict the ultimate flexural strength with good accuracy.

Unbond of steel reinforcement caused a decrease in the ultimate flexural strength due to the decrease in strain in steel rebars at ultimate. This occurred when a bond failure was avoided due to the insignificance of the unbonded length.

When the unbonded portion was long enough to force a bond failure prior to a flexural one, a significant decrease in the ultimate flexural strength and ductility were reported.

CFRP sheets were able to increase the ultimate flexural strength and restore up between 80% and 93% of the original capacity based on the length of unbond.

Despite the fact the CFRP sheets were unable to restore a desirable flexural mode of failure when the unbonded length is relatively large, they were able to increase the mid-span deflection by 10% and 73% for BU28 and BU30, respectively.

**Notation**

- $A_s$  = area of tensile steel reinforcement
- $A'_s$  = area of compressive steel reinforcement
- $b$  = width of the cross-section
- $c$  = distance from extreme fibres in compression to the neutral axis
- $C_c$  = the total compressive force of concrete at the critical section
- $C_s$  = the total compressive force of compressive steel at the critical section
- $d$  = distance from extreme fibres in compression to the centroid of tensile reinforcement
- $d'$  = distance from extreme fibres in compression to the centroid of compressive reinforcement
- $d_0$  = diameter of reinforcing bar
- $E_c$  = modulus of elasticity of concrete
- $E_s$  = modulus of elasticity of steel
- $f_c$  = concrete compressive strength at strain  $\epsilon$
- $f'_c$  = specified compressive strength of concrete
- $f_y$  = yield strength of tensile steel
- $f_{yc}$  = yield strength of compression steel
- $f_{yc}$  = yield strength of compressive steel
- $h$  = overall depth of the concrete cross-section
- $i$  = variable accounts for the number of iterations
- $l_e$  = the element length in ANSYS

- $L$  = span of beam
- $L_{CFRP}$  = length of beam wrapped with CFRP sheets
- $L_{ub}$  = length of the beam over which reinforcement is unbonded
- $M_n$  = calculated ultimate bending strength of RC beams with perfectly bonded steel
- $N$  = number of tensile reinforcing bars
- $P_{u(Anal.)}$  = the calculated analytical value of ultimate load
- $P_{u(FEA)}$  = calculated FEA value of ultimate load
- $P_{u(ex p.)}$  = the calculated experimental value of ultimate load
- $S$  = the span of the beam
- $T$  = total yield force of tensile steel at the critical section
- $T_y$  = yield force of tensile steel at the critical section
- $y$  = distance from extreme compression fibres to the centroid of concrete in compression
- $\epsilon$  = concrete strain corresponding to concrete compressive strength  $f_c$
- $\epsilon_{cx}$  = the strain of concrete adjacent to steel rebars in the unbonded region at a distance  $x$  from the end of the beam
- $\epsilon_{cu}$  = the ultimate compressive strain of concrete
- $\epsilon_s$  = strain of tensile perfectly bonded steel reinforcement
- $\epsilon_{sc}$  = the strain of compressive steel reinforcement
- $\epsilon_{sub}$  = the strain of tensile unbonded steel reinforcement
- $\epsilon_y$  = yield strain of tensile steel reinforcement
- $\epsilon_{yc}$  = yield strain of compressive steel reinforcement
- $\epsilon_0$  = concrete strain corresponding to concrete compressive strength, taken as  $\epsilon_0 = 1.8f'_c/E_c$
- $\delta$  = tolerance adopted in obtaining ultimate flexural strength
- $\delta_{(c)}$  = numerical load step of the depth of neutral axis
- $\delta_{(\epsilon)}$  = numerical load step of strain in concrete at maximum fibre in compression
- $\delta_{(\epsilon_{cu})}$  = numerical load step of the ultimate compressive strain of concrete
- $\tau$  = bond stress at a given point
- $\tau_b$  = peak bond strength values for Pull-out modes of failure
- $\tau_{b,split}$  = peak bond strength values for splitting modes of failure
- $\mu$  = moment reduction factor

## References

- [1] K. Andisheh, et al., "Influence of Chloride Corrosion on the Effective Mechanical Properties of Steel Reinforcement," *Structure and Infrastructure Engineering*, vol. 15, no. 8, pp. 1036–1048, 2019. *Crossref*, <https://doi.org/10.1080/15732479.2019.1594313>
- [2] Ju-Seong Jung, et al., "Experimental Study on the Structural Performance Degradation of Corrosion-Damaged Reinforced Concrete Beams," *Advances in Civil Engineering*, pp. 9562574, 2019. *Crossref*, <https://doi.org/10.1155/2019/9562574>
- [3] Geocisa and the Torroja Institute, Contecvet: A Validated Users Manual for Assessing the Residual Service Life of Concrete Structures. Manual for Assessing Corrosion-Affected Concrete Structures. Annexe {C} Calculation of A Representative Corrosion Rate, Ec Innov. Program. In30902i, Geocisa, Madrid, Spain, No. Ec Innovation Program In309021, 2002.
- [4] George J. Verbeck, "Mechanisms of Corrosion of Steel in Concrete," *ACI Symposium Publications*, vol. 49, pp. 21-38, 1975.
- [5] Aci Committee 318, "318-19 Building Code Requirements for Structural Concrete and Commentary," 2019.
- [6] Alok A. Deshpande, Dhanendra Kumar, and Ravi Ranade, "Temperature Effects on the Bond Behaviour Between Deformed Steel Reinforcing Bars and Hybrid Fibre-Reinforced Strain-Hardening Cementitious Composite," *Construction and Building Materials*, vol. 233, pp. 117337, 2020. *Crossref*, <https://doi.org/10.1016/j.conbuildmat.2019.117337>
- [7] LeHuang et al., "Local Bond Performance of Rebar Embedded in Steel-Polypropylene Hybrid Fibre Reinforced Concrete Under Monotonic and Cyclic Loading," *Construction and Building Materials*, vol. 103, pp. 77–92, 2016. *Crossref*, <https://doi.org/10.1016/j.conbuildmat.2015.11.040>
- [8] Yousef R. Alharbi et al., "Bond Behaviour Between Concrete and Steel Rebars for Stressed Elements," *AIN Shams Engineering Journal*, vol. 12, no. 2, pp. 1231-1239, 2021. *Crossref*, <https://doi.org/10.1016/j.asej.2020.10.001>
- [9] Zemei Wu, Caijun Shi, and Kamal Henri Khayat, "Multi-Scale Investigation of Microstructure, Fibre Pullout Behaviour, and Mechanical Properties of Ultra-High Performance Concrete With Nano-Caco<sub>3</sub> Particles," *Cement and Concrete Composites*, vol. 86, pp. 255–265, 2018. *Crossref*, <https://doi.org/10.1016/j.cemconcomp.2017.11.014>
- [10] I. Minkarah and B. C. Ringo, "Behavior and Repair of Deteriorated Reinforced Concrete Beams," *Transportation Research Record*, vol. 4, pp. 73–79, 1981.
- [11] J. Cairns and Z. Zhao, "Behaviour of Concrete Beams With Exposed Reinforcement," *Proceedings of the Institution of Civil Engineers: Structures and Buildings*, vol. 99, no. 2, pp. 141-154, 1993. *Crossref*, <https://doi.org/10.1680/istbu.1993.23373>
- [12] M. Raoof and Z. Lin, "Structural Characteristics of Rc Beams With Exposed Main Steel," *Proceedings of the Institution of Civil Engineers: Structures and Buildings*, vol. 122, no. 1, pp. 35–51, 1997. *Crossref*, <https://doi.org/10.1680/istbu.1997.29166>
- [13] K. Stanish, "Effects on Bond," *Response*, 1997.
- [14] H. Iemura, Y. Takahashi, and Naoki, "Development of Unbonded Bar Reinforced Concrete Structure," *13th World Conference on Earthquake Engineering*, 2002.
- [15] G. R. Pandey and H. Mutsuyoshi, "Seismic Damage Mitigation of Reinforced Concrete Bridge Piers by Unbonding Longitudinal Reinforcements," *13th World Conference on Earthquake Engineering*, 2002.
- [16] K. S. Tamer El Maaddawy, Khaled Soudki and Timothy Topper, "Long-Term Performance of Corrosion-Damaged Reinforced Concrete Beams," *ACI Structural Journal* vol. 102, no. 5, 649-656, 2005.
- [17] D. N. Smith and L. A. Wood, "21 - the Structural Performance of Damaged Concrete Elements," *The Life of Structures Physical Testing* pp. 181–190, 1989. *Crossref*, <https://doi.org/10.1016/B978-0-408-04245-1.50025-X>
- [18] L. A. C. Yingang Du, Leslie A. Clark and Andrew Hin Cheong Chan, "Impact of Reinforcement Corrosion on Ductile Behavior of Reinforced Concrete Beams," *ACI Structural Journal*, vol. 104, no. 3, pp. 285-293, 2007.
- [19] Fares Jnaid and Riyadh S. Aboutaha, "Residual Flexural Strength of Corroded Reinforced Concrete Beams," *Engineering Structures*, vol. 119, pp. 198–216, 2016.
- [20] G. M. Kotsovos, E. Vougioukas, and M. D. Kotsovos, "Behaviour of Reinforced Concrete Beams With Non-Bonded Flexural Reinforcement," *Magazine of Concrete Research*, vol. 67, no. 10, pp. 503–512, 2015. *Crossref*, <http://dx.doi.org/10.1680/mac.14.00114>
- [21] J. R. Eyre and M. A. Nokhasteh, "Strength Assessment of Corrosion Damaged Reinforced Concrete Slabs and Beams," *Proceedings of the Institution of Civil Engineers: Structures and Buildings*, vol. 94, no. 2, pp. 197–203, 1992. *Crossref*, <https://doi.org/10.1680/istbu.1992.18788>
- [22] W.-L. Wang and Ju Chen, "Residual Strengths of Reinforced Concrete Beams With Heavy Deterioration," *Research Journal of Applied Sciences, Engineering and Technology*, vol. 3, no. 8, pp. 798–805, 2011.
- [23] F. J. and R. S. Aboutaha, "Residual Flexural Strength of Rc Beams With Unbonded Reinforcement," *ACI Structural Journal*, vol. 111, no. 6. *Crossref*, <http://dx.doi.org/10.14359/51686975>
- [24] A. M. Jadhav and H. K. Munot, "Analytical Study of Mechanism of Concrete Cracking and Its Propagation Due to Corrosion of Reinforcement in RCC," *The Open Civil Engineering Journal*, vol. 6, no. 2, pp. 286–294, 2016. *Crossref*, <http://dx.doi.org/10.4236/ojce.2016.62024>
- [25] "ACI 408r-03 Bond and Development of Straight Reinforcing Bars in Tension," *ACI Committee 408*, 2003.

- [26] Eligehausen, Rolf, Popov, Egor P., and Bertero, Vitelmo V, "Local Bond Stress-Slip Relationships of Deformed Bars Under Generalized Excitations," *Experimental Results and Analytical Model*, 1983. *Crossref*, <http://dx.doi.org/10.18419/opus-415>
- [27] Filip C. Filippou, Egor P. Popov, and Vitelmo V. Bertero, "Effects of Bond Deterioration on Hysteretic Behaviour of Reinforced Concrete Joint (EERC 83-19), *Earthquake Engineering Research Center*, University of California, Berkeley, pp. 212, 1983.
- [28] M. Esfahani, and B. Rangan, "Local Bond Strength of Reinforcing Bars in Normal Strength and High-Strength Concrete (HSC)," *ACI Structural Journal*, vol. 95, no. 2, pp. 96-106, 1998.
- [29] M. Esfahani, and B. Rangan "Bond Between Normal Strength and High-Strength Concrete (HSC) and Reinforcing Bars in Splices in Beams," *ACI Structural Journal* , vol. 95, no. 3, pp. 272-280, 1998.
- [30] Mohamed H. Harajli, "Comparison of Bond Strength of Steel Bars in Normal- and High-Strength Concrete," *Journal of Materials in Civil Engineering*, vol. 16, no. 4, pp. 365–374, 2004. *Crossref*, [http://dx.doi.org/10.1061/\(ASCE\)0899-1561\(2004\)16:4\(365\)](http://dx.doi.org/10.1061/(ASCE)0899-1561(2004)16:4(365))
- [31] Mohamed H. Harajli, "Bond Stress–Slip Model for Steel Bars in Unconfined Or Steel, Frc, Or Frp Confined Concrete Under Cyclic Loading," *Journal of Structural Engineering*, vol. 135, no. 5, pp. 509–518, 2009. *Crossref*, [http://dx.doi.org/10.1061/\(ASCE\)0733-9445\(2009\)135:5\(509\)](http://dx.doi.org/10.1061/(ASCE)0733-9445(2009)135:5(509))
- [32] Mohamed H. Harajli. and M. E. Mabsout, "Evaluation of Bond Strength of Steel Reinforcing Bars in Plain and Fiber-Reinforced Concrete," *ACI Structural Journal*, vol. 99, no. 4, pp. 509-517, 2002.
- [33] Fib, Model Code 2010, 2011.
- [34] S. Coccia, E. Di Maggio, and Z. Rinaldi, " Bond Slip Model in Cylindrical Reinforced Concrete Elements Confined With Stirrups," *International Journal of Advanced Structural Engineering*, vol. 7, no. 4, pp. 365–375, 2015. *Crossref*, <https://doi.org/10.1007/s40091-015-0104-7>
- [35] Weiping Zhao, and Binrong Zhu, "Theoretical Model for the Bond-Slip Relationship Between Ribbed Steel Bars and Confined Concrete," *Structural Concrete*, vol. 19, no. 11, pp. 548–558, 2018. *Crossref*, <https://doi.org/10.1002/suco.201700008>
- [36] Y. Zhao and H. Lin, "The Bond Behaviour Between Concrete and Corroded Reinforcement: State of the Art," *6<sup>th</sup> The International Conference on the Durability of Concrete Structures- ICDCS*, pp. 63–73, 2018.
- [37] S. H. Chu and A. K. H. Kwan, "A New Bond Model for Reinforcing Bars in Steel Fibre Reinforced Concrete," *Cement and Concrete Composites*, vol. 104 , pp. 103405, 2019. *Crossref*, <https://doi.org/10.1016/j.cemconcomp.2019.103405>
- [38] P. V. V. Hota , V. S. Gangarao, "Bending Behavior of Concrete Beams," *The Journal of Structural Engineering*, vol. 6 , pp. 3–10, 1998.
- [39] Rami A. Hawileh, et al., "Behavior of Reinforced Concrete Beams Strengthened With Externally Bonded Hybrid Fibre Reinforced Polymer Systems," *Materials and Design*, vol. 53, pp. 972–982, 2014. *Crossref*, <https://doi.org/10.1016/j.matdes.2013.07.087>
- [40] "Aci 440.2r-17: Guide for the Design and Construction of Externally Bonded Frp Systems for Strengthening Existing Structures," *ACI Committee 440*. 2017.

## Figures

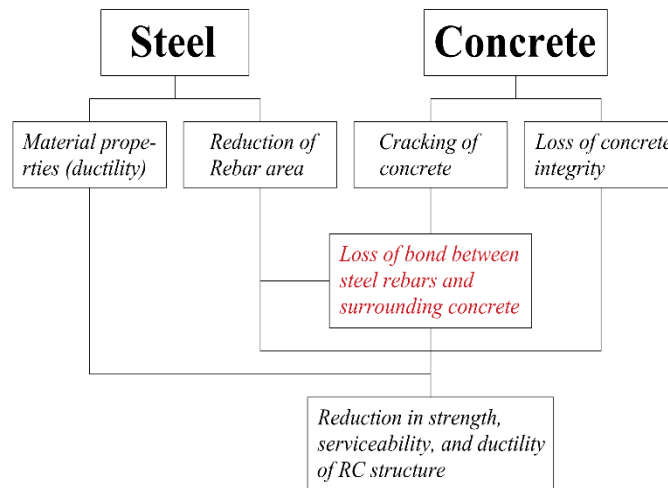


**Fig. 1 Consequences of corrosion on structural performance (after [3]).**

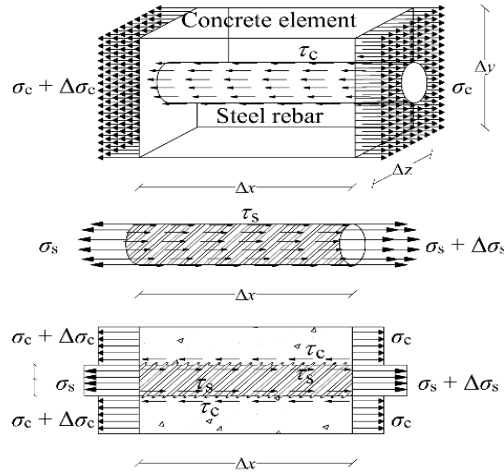


Fig. 2 Stress transfer between concrete and steel rebars.

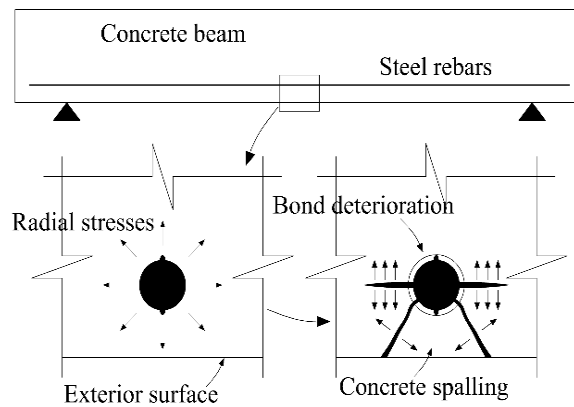


Fig. 3 Effect of corrosion of reinforcing steel bars on the surrounding concrete.

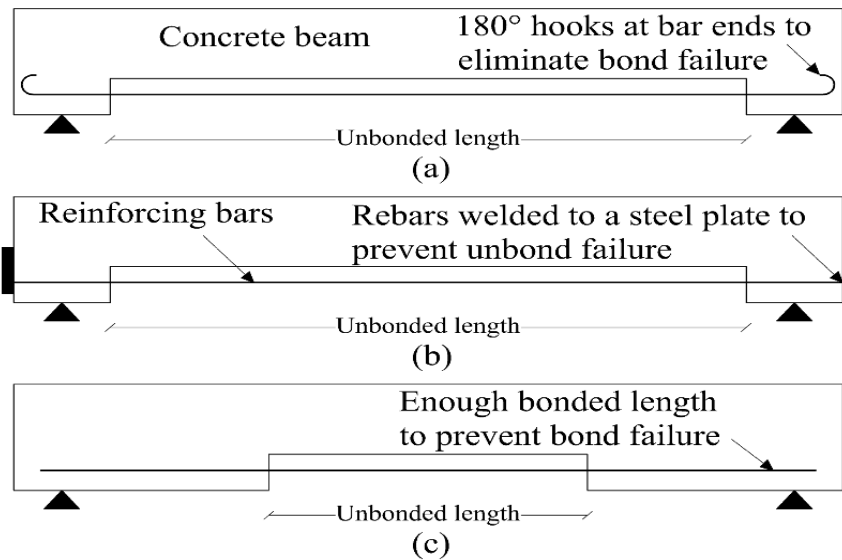


Fig. 4 Securing bond between concrete beams and embedded reinforcement: (a) hooks at rebar ends; (b) welding rebars' ends to a steel plate, and (c) providing enough bonded length to eliminate a bond failure.

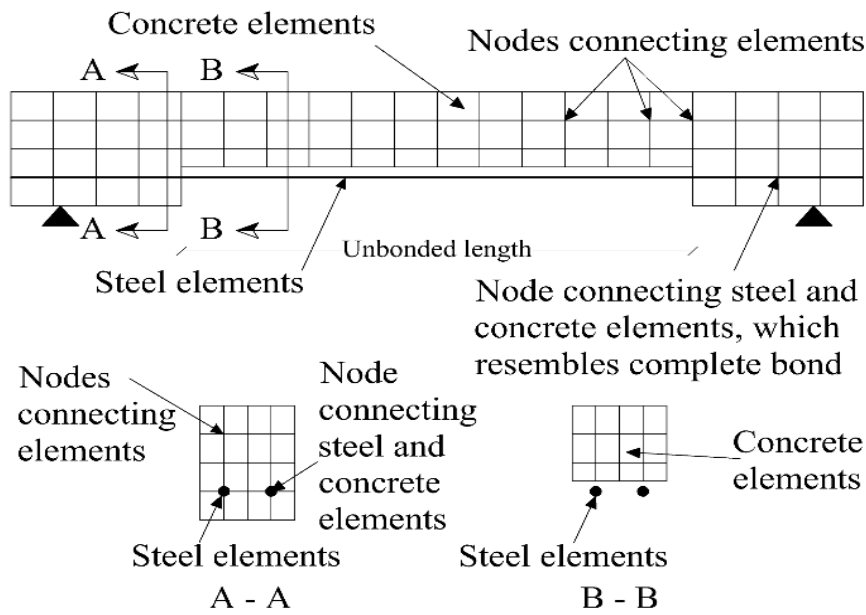


Fig. 5 Connecting steel and concrete elements to the same nodes to eliminate bond failure.

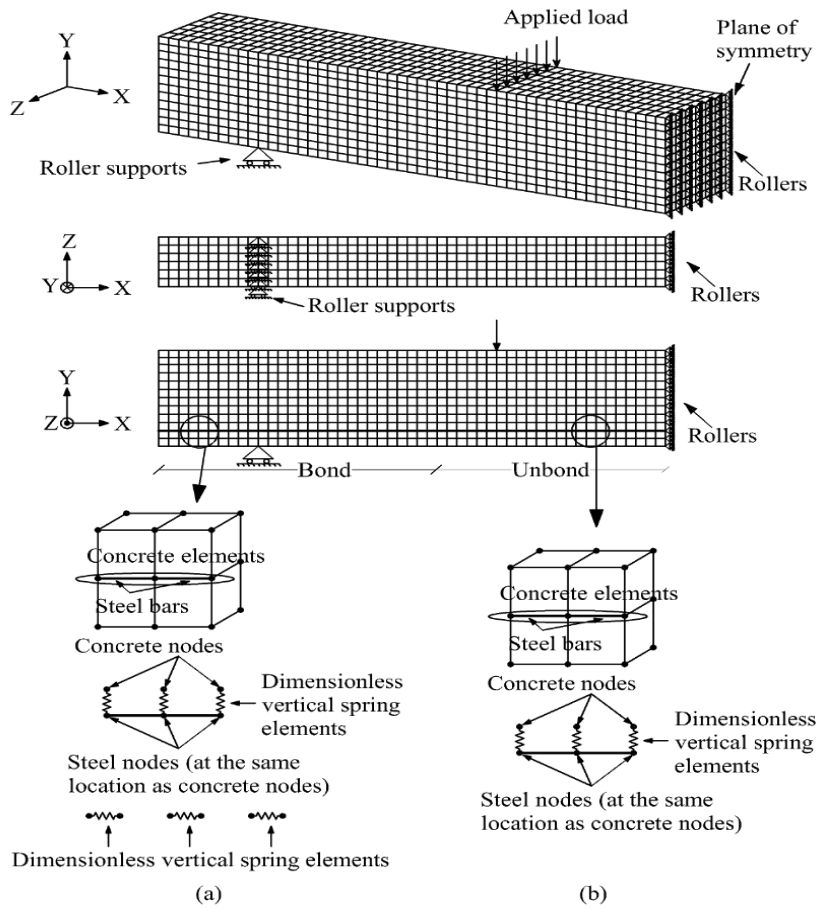


Fig. 6 Modelling of a) bond between steel rebars and adjacent concrete and b) unbond between steel rebars and adjacent concrete

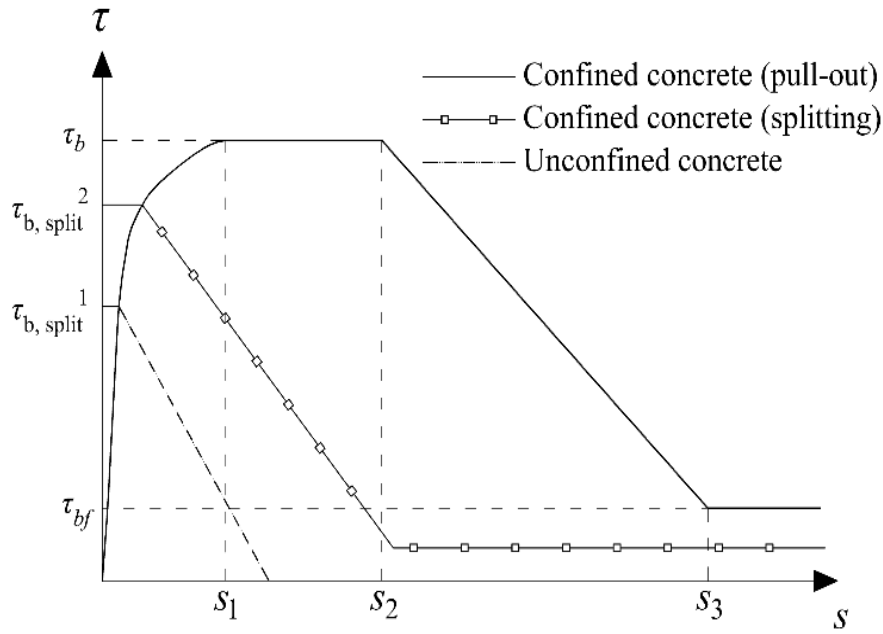


Fig. 7 Analytical monotonic bond stress-slip curves (after Fib Model Code 2010).

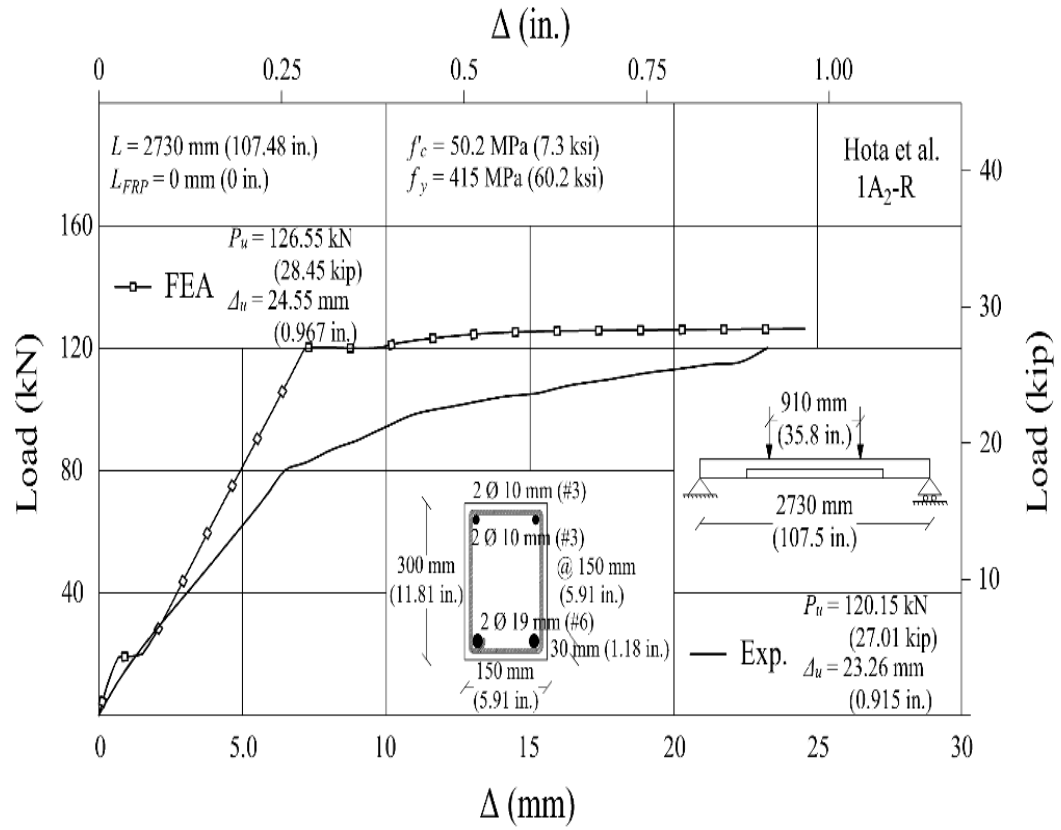


Fig. 8 Load-deflection curve FEA vs experimental (1A2-R)

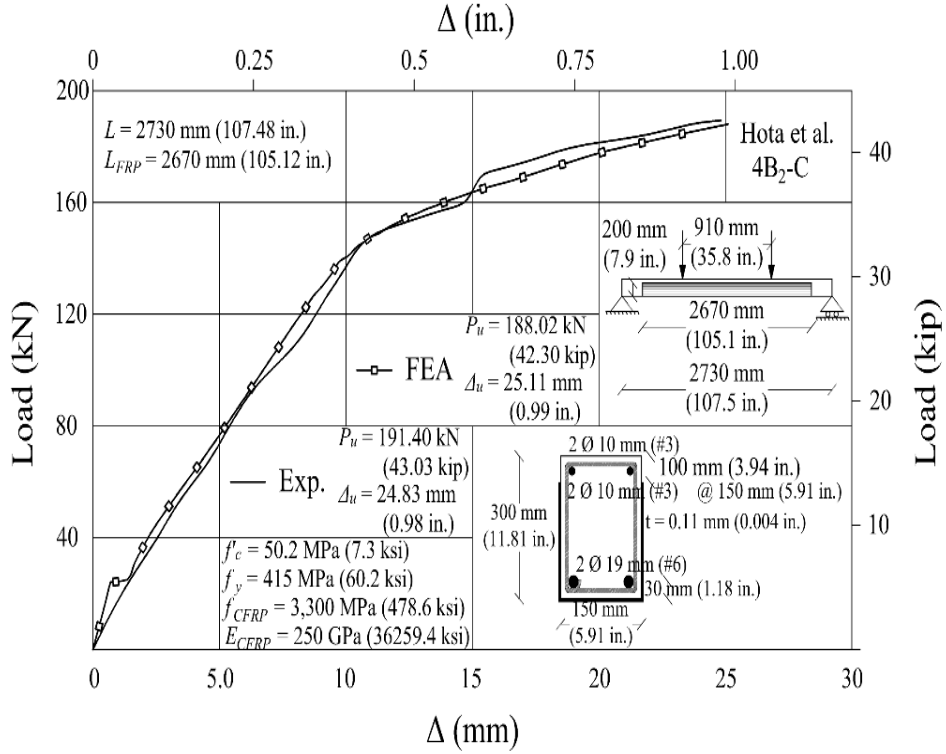


Fig. 9 Load-deflection curve FEA vs experimental (4B<sub>2</sub>-C)

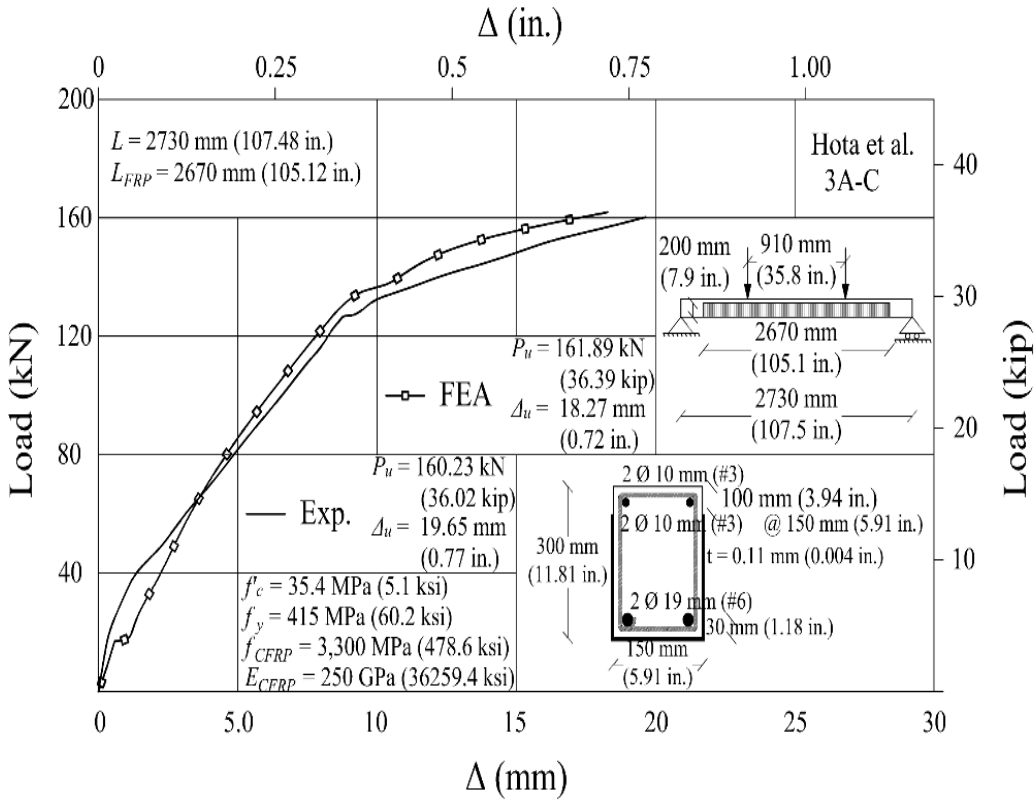


Fig. 10 Load-deflection curve FEA vs experimental (3A-C)

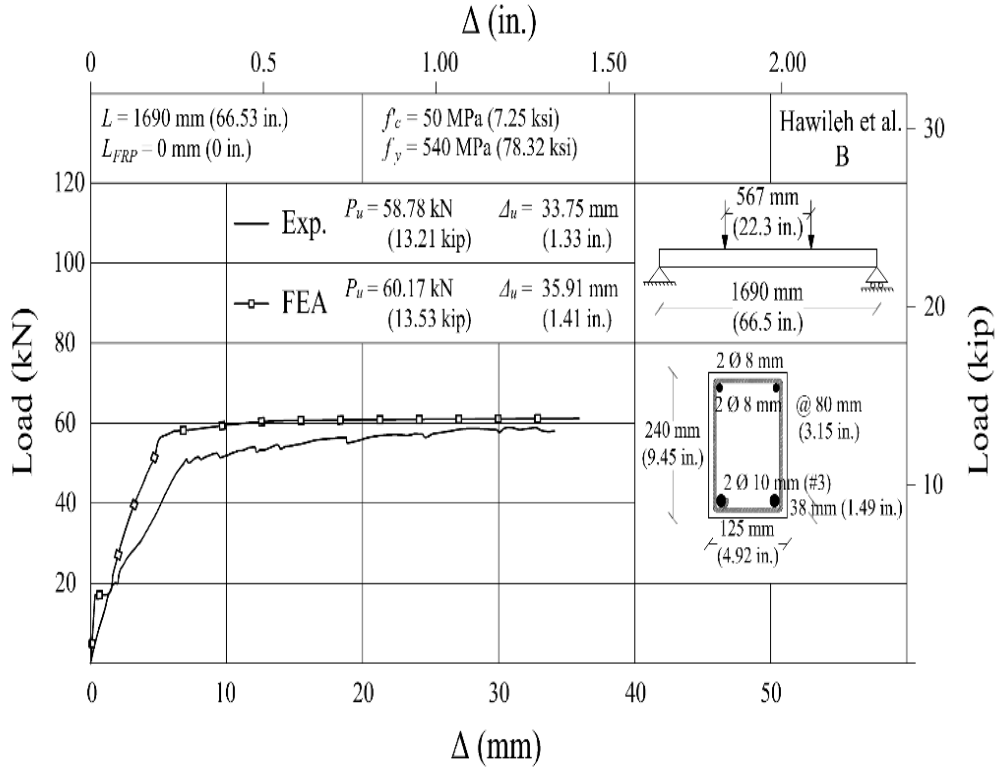


Fig. 11 Load-deflection curve FEA vs experimental (B)

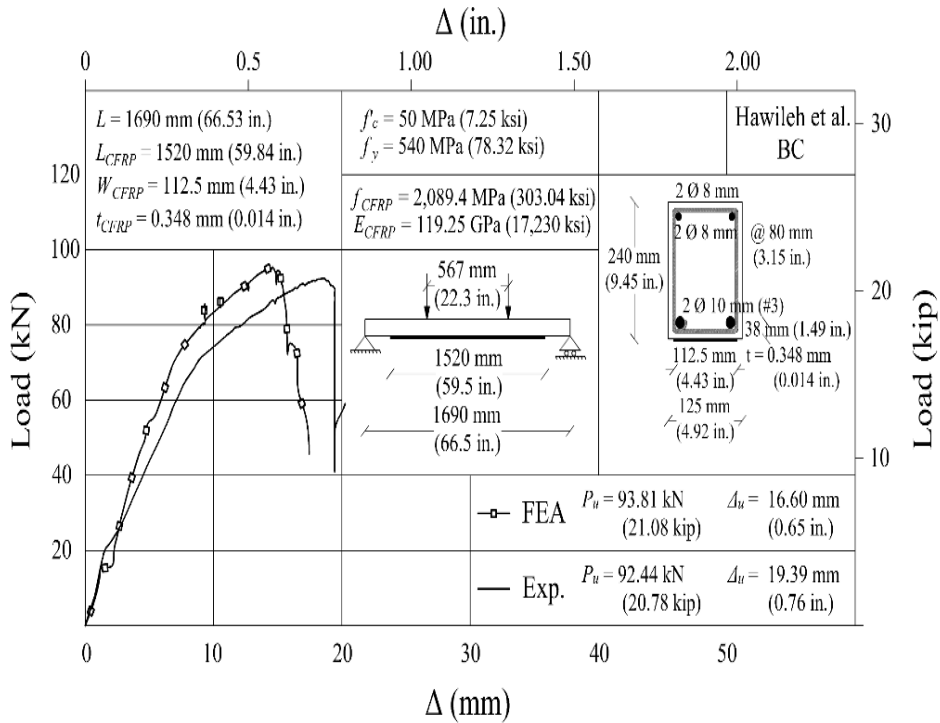


Fig. 12 Load-deflection curve FEA vs experimental (BC)

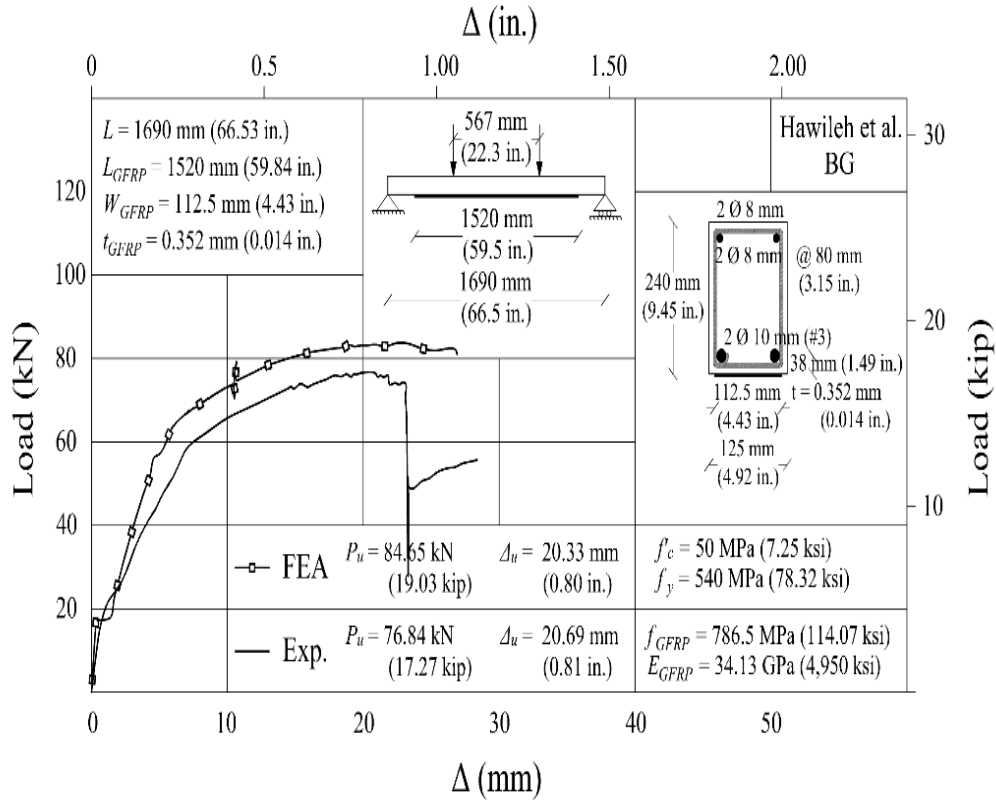


Fig. 13 Load–deflection curve FEA vs experimental (BG)

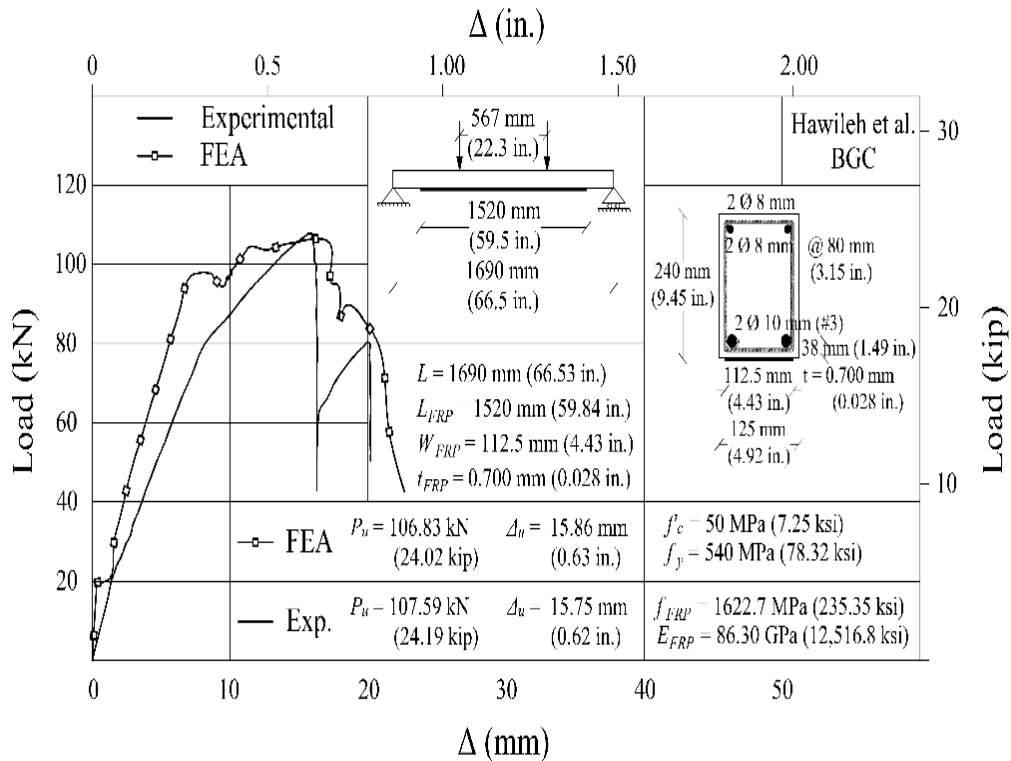


Fig. 14 Load–deflection curve FEA vs experimental (BGC)

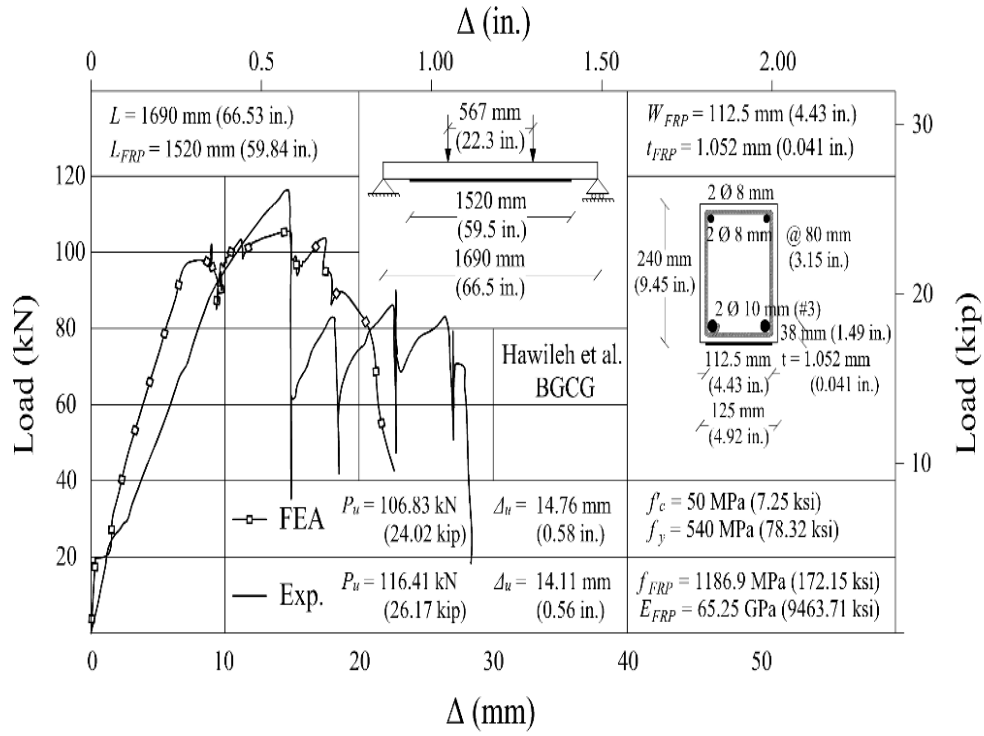


Fig. 15 Load-deflection curve FEA vs experimental (BGCG)

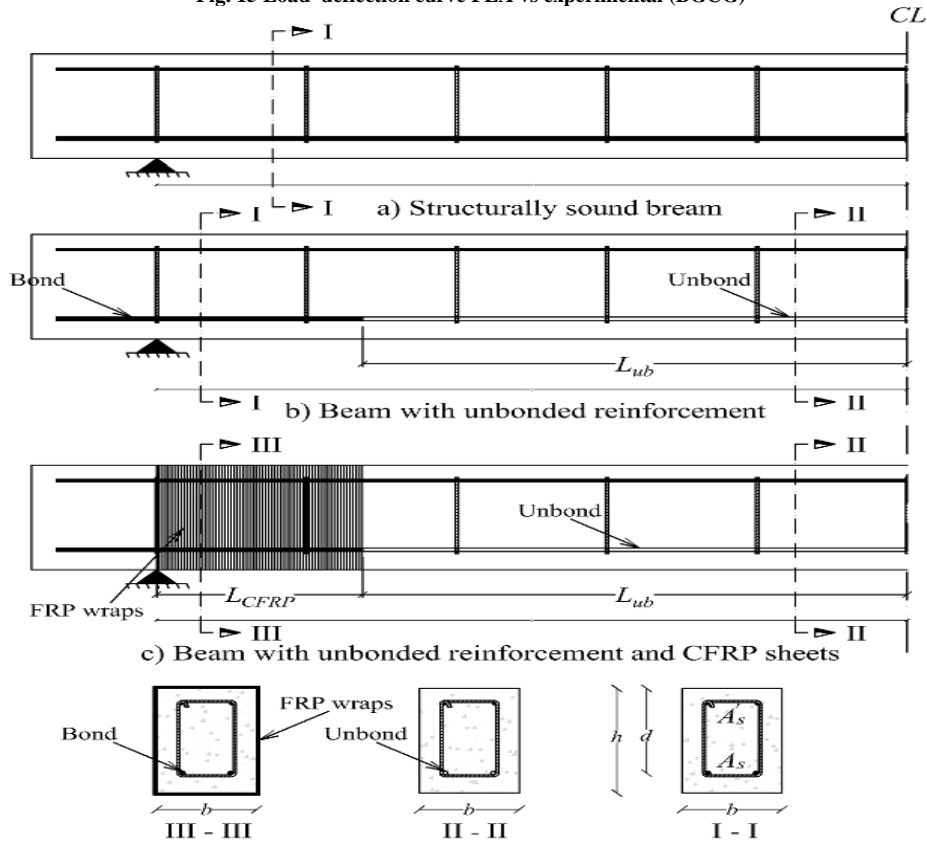


Fig. 16 Applications of CFRP sheets on unbonded beams.

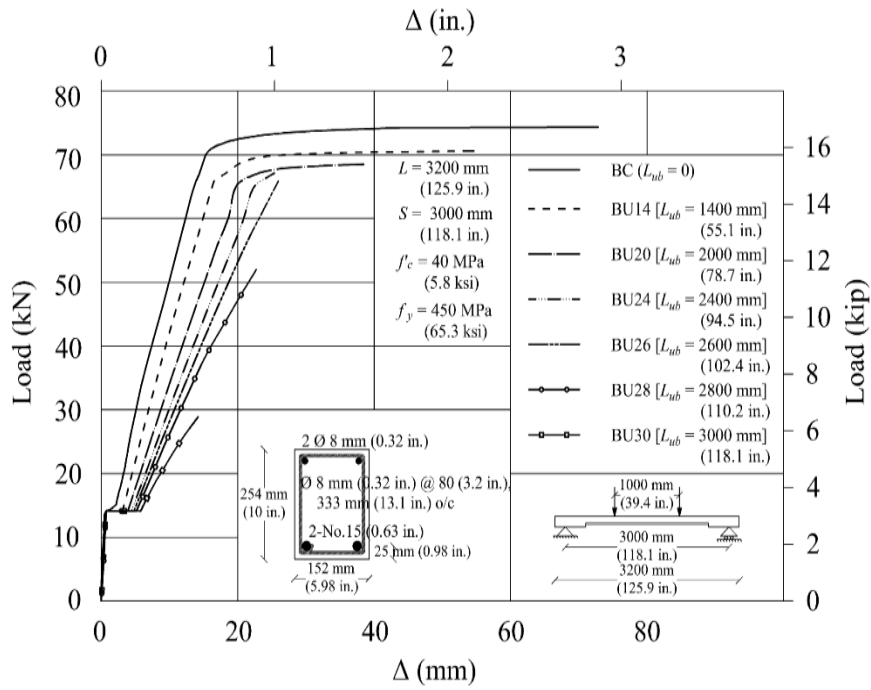
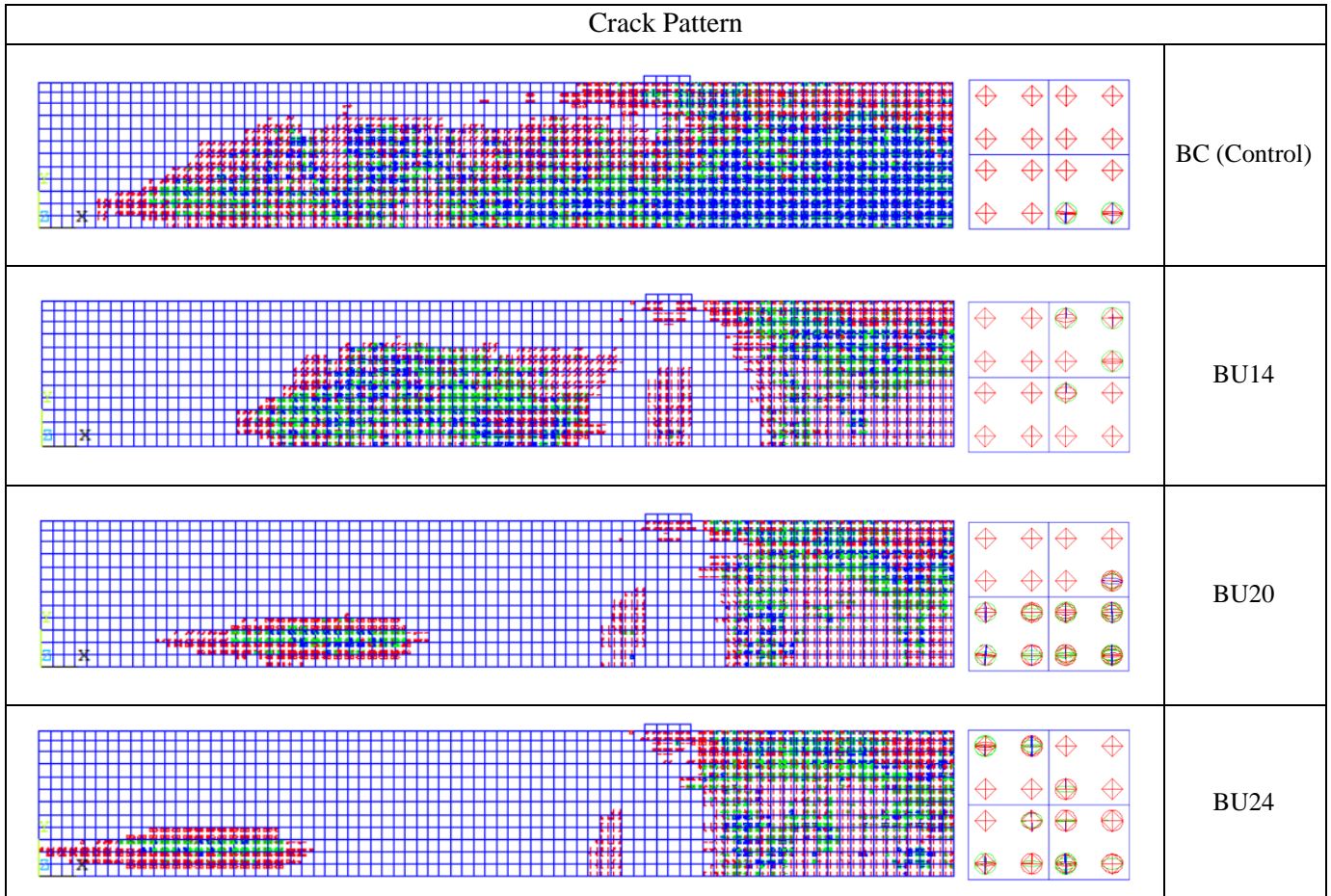


Fig. 17 Load–deflection curves of beams with various unbonded lengths



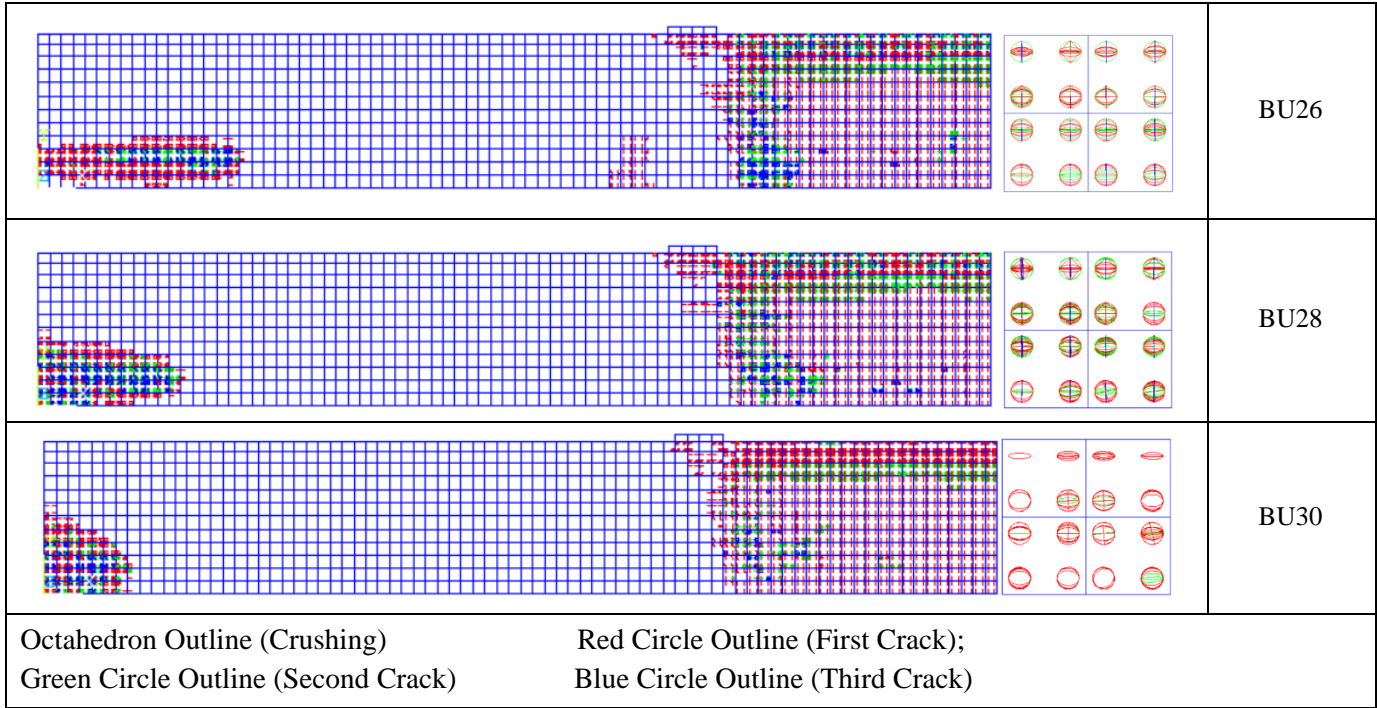


Fig. 18 Crack patterns for beams with different unbonded lengths at ultimate

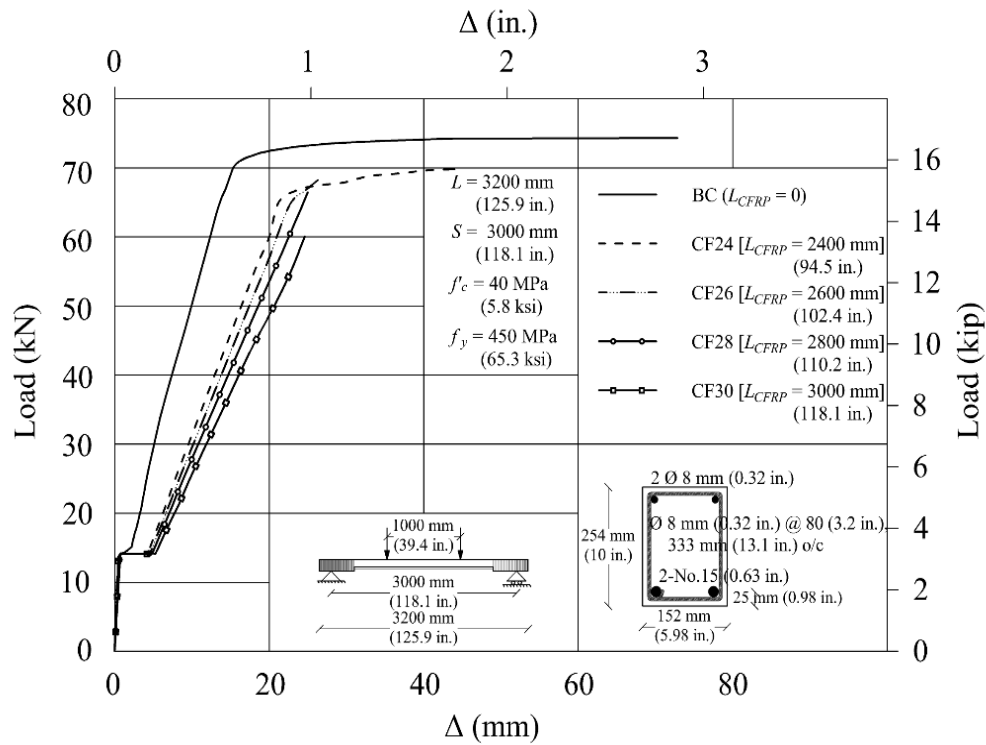


Fig. 19 Load-deflection curves of beams strengthened with CFRP sheets

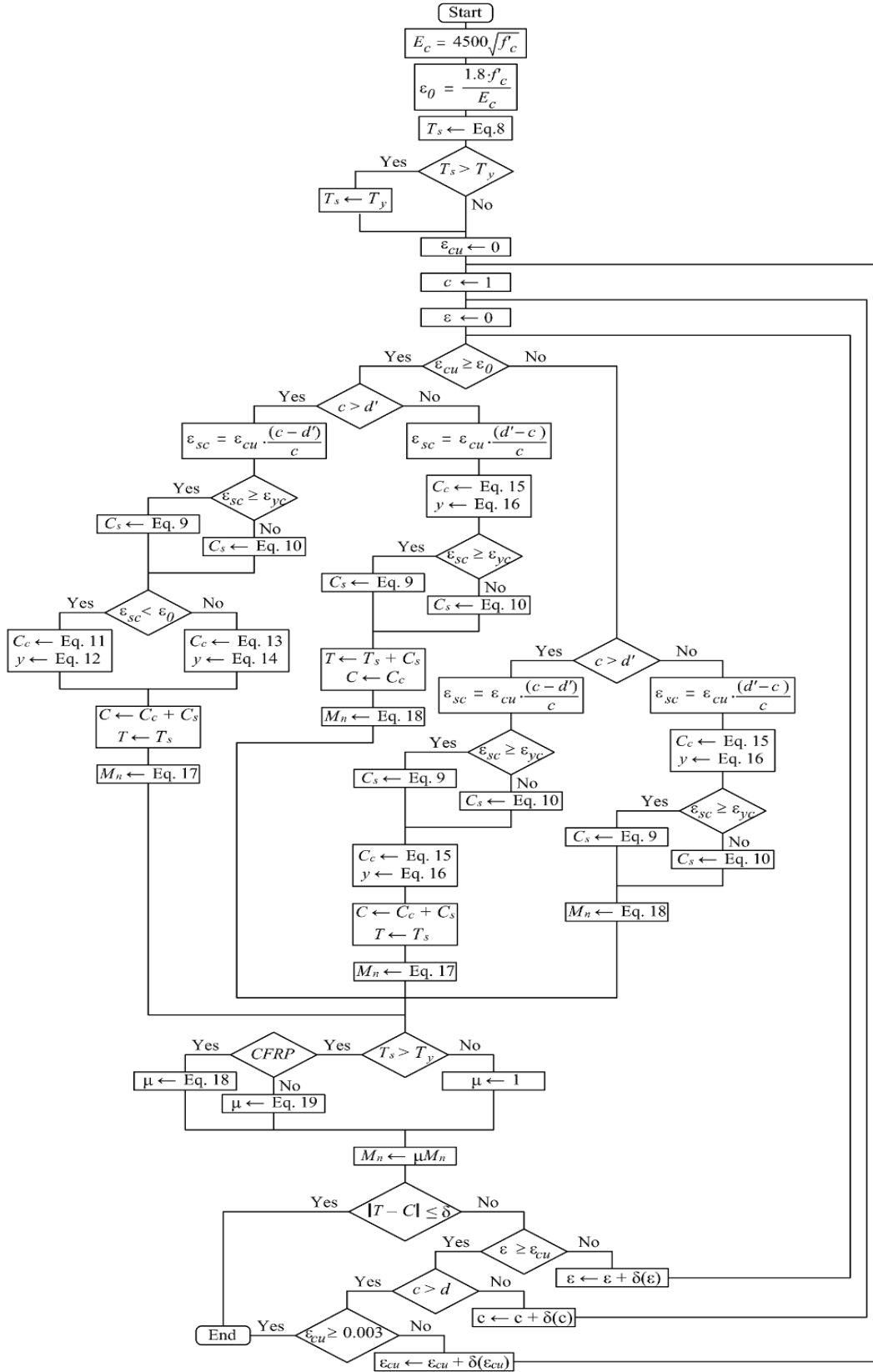


Fig. 20 Flowchart of the analytical procedure

**Appendix A**

Material	Concrete	
Type	SOLID65	
No. of elements	5,760	
No. of nodes for each element	8	
Linear isotropic	Modulus of Elasticity	30,042 MPa (4,357 ksi)
	Poisson's ratio	0.2
Multilinear isotropic	Stress-strain diagram	modified Hognestad
Concrete	Open shear transfer coefficient	0.3
	Closed shear transfer coefficient	1
	Uniaxial cracking stress	3.4 MPa (0.5 ksi)
	Uniaxial crushing stress	40 MPa (5.8 ksi)
Material	Steel Bars	
Type	LINK180	
No. of elements	656 (including tension, compression, and stirrups)	
No. of nodes for each element	2	
Linear isotropic	Modulus of Elasticity	200,000 MPa (29,000 ksi)
	Poisson's ratio	0.3
Bilinear isotropic	Yield stress	450 MPa (58 ksi)
	Tangent modulus	0
Real constants	Cross-section area (tensile reinforcement)	201 mm <sup>2</sup> (0.31 in <sup>2</sup> )
	Initial strain (tensile reinforcement)	0 mm/mm (0 in/in)
	Cross-section area (compressive reinforcement)	50.3 mm <sup>2</sup> (0.08 in <sup>2</sup> )
	Initial strain (compressive reinforcement)	0 mm/mm (0 in/in)
	Cross-section area (stirrups)	50.3 mm <sup>2</sup> (0.08 in <sup>2</sup> )
	Initial strain (stirrups)	0 mm/mm (0 in/in)
Material	Steel Plate	
Type	SOLID185	
No. of elements	24	
No. of nodes for each element	8	
Linear isotropic	Modulus of Elasticity	200,000 MPa (29,000 ksi)
	Poisson's ratio	0.3
Bilinear isotropic	Yield stress	450 MPa (58 ksi)
	Tangent modulus	0
Material	Vertical Spring Elements	
Type	COMBIN14	
No. of elements	Varies	
No. of nodes for each element	2	
Real constants	Spring stiffness	10 <sup>6</sup> N/mm (571 kip/in.)
	Initial force	0
	Damping coefficients	0
Material	Horizontal Spring Elements	
Type	Combin39	
No. of elements	Varies	
No. of nodes for each element	2	
Real constants	Spring stiffness	Load-deflection curve
	Initial force	0
	Damping coefficients	0

Material	Epoxy Resin	
Type	SOLID65	
No. of elements	Varies	
No. of nodes for each element	8	
Linear isotropic	Modulus of Elasticity	4,500 MPa (653 ksi)
	Poisson's ratio	0.33
Multilinear Elastic	Stress-strain diagram	60 MPa (8.7 ksi) 0.013
Material	CFRP	
Type	SOLID185	
No. of elements	Varies	
No. of nodes for each element	8	
Linear orthotropic	EX	230,000 MPa (33386 ksi)
	EY	4,500 MPa (653 ksi)
	EZ	4,500 MPa (653 ksi)
	PRXY	0.4
	PRYZ	0.3
	PRXZ	0.4
	GXY	82,142 MPa (11,914 ksi)
	GYZ	1,731 MPa (251 ksi)
	GXZ	82,142 MPa (11,914 ksi)
Multilinear Elastic	Stress strain diagram	3,790 MPa (550 ksi) 0.017

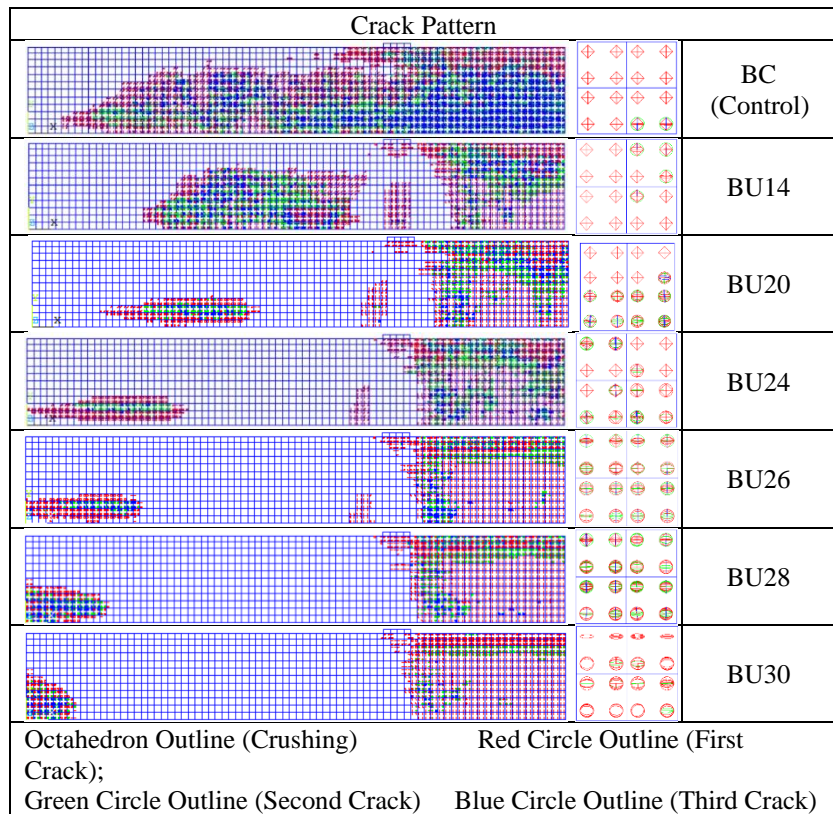
### Appendix B

	Confined				Unconfined	
	$\varepsilon_s < \varepsilon_y$				$\varepsilon_s < \varepsilon_y$	
	Pull-out (PO)		Splitting (SP)		Splitting (SP)	
	Good bond	other	Good bond	other	Good bond	other
$\tau_b$	$2.5\sqrt{f'_c}$	$1.25\sqrt{f'_c}$				
$\tau_{b,split}$			$8 \cdot \left[\frac{f'_c}{25}\right]^{0.25}$	$5.5 \cdot \left[\frac{f'_c}{25}\right]^{0.25}$	$7 \cdot \left[\frac{f'_c}{25}\right]^{0.25}$	$5 \cdot \left[\frac{f'_c}{25}\right]^{0.25}$
$\tau_{bf}$	$0.40\tau_b$	$0.40\tau_b$	$0.40\tau_{b,split}$	$0.40\tau_{b,split}$	0	0
$s_1$	1.0 mm	1.8 mm	$s(\tau_{b,split})$	$s(\tau_{b,split})$	$s(\tau_{b,split})$	$s(\tau_{b,split})$
$s_2$	2.0 mm	3.6 mm	$s_1$	$s_1$	$s_1$	$s_1$
$s_3$	$c_{clear} *$	$c_{clear} *$	$0.5c_{clear} *$	$0.5c_{clear} *$	$1.2s_1$	$1.2s_1$
$a$	0.4	0.4	0.4	0.4	0.4	0.4
$c_{clear} *$ is the clear distance between ribs (1 MPa = 145 psi)						

**Appendix C**

ANSYS vs Exp.	Specimen reference	$f'_c$ MPa (ksi)	$f_y$ MPa (ksi)	$L$ mm (in.)	$L_{FRP}$ mm (in.)	$P_{u(exp.)}$ kN (kip)	$P_{u(FEA)}$ kN (kip)	$P_{u(exp.)}/P_{u(FEA)}$
Hota <i>et al.</i> [38]	1A <sub>2</sub> -R	50.2 (7.3)	415 (60.2)	2730 (107.48)	0	120.15 (27.01)	126.55 (28.45)	0.95
	4B <sub>2</sub> -C	50.2 (7.3)	415 (60.2)	2730 (107.48)	2670 (105.12)	191.40 (43.03)	188.02 (42.30)	1.02
	3A-C	35.4 (5.1)	415 (60.2)	2730 (107.48)	2670 (105.12)	161.89 (36.39)	160.23 (36.02)	1.01
Hawileh <i>et al.</i> [39]	B	50 (7.3)	540 (78.3)	1690 (66.54)	0	58.78 (13.21)	60.17 (15.53)	0.98
	BC	50 (7.3)	540 (78.3)	1690 (66.54)	1520 (59.84)	92.44 (20.78)	93.44 (21.08)	0.99
	BG	50 (7.3)	540 (78.3)	1690 (66.54)	1520 (59.84)	76.84 (17.27)	84.65 (19.03)	0.91
	BGC	50 (7.3)	540 (78.3)	1690 (66.54)	1520 (59.84)	107.59 (24.19)	106.83 (24.02)	1.01
	BCGC	50 (7.3)	540 (78.3)	1690 (66.54)	1520 (59.84)	116.41 (26.17)	106.83 (24.02)	1.09
							Mean	0.99
							Sta. Dev.	0.05

**Appendix D**



**Appendix E**

	$L_{ub}$ mm	$L_{CFRP}$ mm	Elastic strain in steel rebars at mid-span ( $\times 10^{-3}$ )	Plastic strain in steel rebars at mid-span ( $\times 10^{-3}$ )	$P_{u(FEA)}$ kN	$P_{u(Anal.)}$ kN	$P_{u(exp.)}/P_{u(FEA)}$	Failure Mode
BC	0	0	2.25	7.56	74.31	73.90	0.9945	1
BU14	1400	0	2.25	2.026	70.60	70.74	1.0020	1
BU20	2000	0	2.25	0.80597	68.50	68.40	0.9985	1
BU24	2400	0	2.1685	0.71459	67.10	66.87	0.9966	1
BU26	2600	0	2.124	0	65.84	66.13	1.0043	2
BU28	2800	0	1.4538	0	51.98	53.31	1.0256	2
BU30	3000	0	0.83039	0	28.88	28.03	0.9706	2
CF24	2400	400	2.25	0.88439	69.11	66.88	0.9678	1
CF26	2600	300	2.25	0.067	68.24	68.39	1.0023	1
CF28	2800	200	1.7374	0	66.45	66.60	1.0023	2
CF30	3000	100	1.5863	0	60.04	66.00	1.0993	2
Mean							1.0058	
Standard Deviation							0.0332	
Notes: 1 mm = 0.0394 in.; 1 kN = 0.2248 kip 1 = Flexural Failure 2 = Bond Failure								